

Article

Microfluidic Approach for Lead Halide Perovskite Flexible Phototransistors

Fatemeh Khorramshahi *  and Arash Takshi 

Department of Electrical Engineering, University of South Florida (USF), Tampa, FL 33620, USA; atakshi@usf.edu

* Correspondence: khorramshahi@usf.edu

Received: 28 September 2020; Accepted: 3 November 2020; Published: 5 November 2020



Abstract: Lead halide perovskites possess outstanding optical characteristics that can be employed in the fabrication of phototransistors. However, due to low current modulation at room temperature, sensitivity to the ambient environment, lack of patterning techniques and low carrier mobility of polycrystalline form, investigation in perovskite phototransistors has been limited to rigid substrates such as silicon and glass to improve the film quality. Here, we report on room temperature current modulation in a methylammonium lead iodide perovskite (MAPbI₃) flexible transistor made by an extremely cheap and facile fabrication process. The proposed phototransistor has the top-gate configuration with a lateral drain–channel–source structure. The device performed in the linear and saturation regions both in the dark and under white light in different current ranges according to the illumination conditions. The transistor showed p-type transport characteristics and the field effect mobility of the device was calculated to be $\sim 1.7 \text{ cm}^2 \text{ V}^{-1} \text{ s}^{-1}$. This study is expected to contribute to the development of MAPbI₃ flexible phototransistors.

Keywords: perovskite; laser engraving; phototransistor

1. Introduction

Advanced applications of transistors for portable and wearable devices require the use of lightweight flexible substrates. Different technologies and materials have been employed to develop flexible phototransistors by low-temperature fabrication methods [1]. Among the materials that are compatible with low-temperature processes, organic semiconductors suffer from low mobility [2] and metal oxide semiconductors require complicated and costly deposition techniques for producing high quality films [3].

An excellent candidate to be used as the photoactive layer in phototransistors is metal halide perovskite. Over the past ten years, metal halide perovskites, and particularly MAPbI₃, have been recognized as the fastest growing technology in solar cell applications. The widespread research into MAPbI₃ photovoltaics is due to its outstanding optical properties, including a high absorption coefficient [4] and low intrinsic recombination rate [5], along with low-cost solution-based fabrication methods [6].

MAPbI₃ is a semiconductor with a direct bandgap of about 1.55–1.65 eV [7], suitable for visible light absorption. MAPbI₃ in its single crystal form has a mobility higher than $100 \text{ cm}^2 \text{ V}^{-1} \text{ s}^{-1}$ [8]. Although many efforts have been devoted to the fabrication of MAPbI₃-based solar cells [9] and light emitting diodes (LEDs) [10], MAPbI₃ photo-transistors are still immature [11].

The feasibility of making MAPbI₃-based transistors has shown before [10,12–27]. Most of the fabricated devices used a Si wafer and a layer of SiO₂ as the gate and the dielectric layer to make a bottom-gate transistor [13,17]. Spin coating of MAPbI₃ on the gate dielectric results in a polycrystalline layer that presents the triode and saturation current–voltage (I–V) response in the transistor only at low temperatures (<200 K) [10,21]. The poor field effect in the devices operated at room temperature is

likely due to the weak bonds between the cations and iodide anion that would generate defects in the semiconductor under an external biasing [10]. The weak bonds also affect the stability of MAPbI₃ and result in hysteresis loops in the I–V characteristic [10]. Three approaches have been followed to obtain room temperature operation. A common approach is to mix MAPbI₃ with an organic semiconductor, graphene, or carbon nanotube (CNT) to make hybrid semiconductors [13,17,25]. This method sacrifices the excellent optical absorption and low recombination rate in pure perovskites. In another approach, dual halide perovskites of MAPbBr_αI_(3-α) or MAPbCl_αI_(3-α) were used instead of MAPbI₃ to make more stable devices [28,29]. However, our earlier studies show that the photoelectric response of dual halide perovskites is much weaker than MAPbI₃ [30]. Another approach to achieve higher stability is to make transistors from single crystals of MAPbI₃ [26]. In this work, we have developed a new fabrication method that has previously tested for making perovskite-based photoresistors with no hysteresis effect and high stability of the device at room temperature [30–33].

In the new fabrication method, instead of using a thin-film design, a laser engraving method is applied to first make a microchannel across two conductive electrodes that later became the drain and source contacts. The microchannel was filled with a solution containing the perovskite precursors. The sample was dried to get a polycrystalline of MAPbI₃. We have found that leaving the sample in vacuum for at least 24 h before coating the perovskite with a layer of a dielectric (i.e., CYTOP) improves the stability of the device significantly [33]. In this work, we used the CYTOP layer as the gate dielectric to make the transistor. Fabricating the device on a polyethylene terephthalate (PET) substrate, the final photodetector was mechanically flexible. The results of the studied device in this work is promising for further investigation of flexible sensors.

2. Materials and Methods

Perovskite precursor was prepared by mixing 0.5 M PbI₂ (98.5%, Alfa Aesar, Haverhill, MA, USA) and 0.5 M MAI (Lumtec, New Taipei City, Taiwan) in GBL (99%, Aldrich, St. Louis, CA, USA) and keeping it on the hotplate at 60 °C overnight. The sample was fabricated using 1 cm × 1 cm piece of indium tin oxide (ITO) coated (thickness of ~300 nm) sheet (60 Ωsq, Sigma-Aldrich). A 200 μL of poly methyl methacrylate (PMMA) in chlorobenzene (0.369 g in 3 mL chlorobenzene) was spin-coated at 1000 rpm for 40 s. This layer (thickness of ~1 μm) was used as an isolating layer between ITO (drain and source contact material) and the gate contact.

After chlorobenzene was evaporated, the sample was laser engraved (Epilog Fusion M2, 60 W) at the power of 0.6 W, speed of 38.1 mm s⁻¹ and pulse per inch (PPI) of 5000. The depth of the engraved channel was ~40 μm. Then the laser engraved channel was filled with 2 μL of the perovskite precursor solution using the capillary force when a droplet of the solution was placed at one end of the channel. The sample was placed on the hotplate at 85 °C for 6 min.

After that, for making the gate dielectric, a 50 μL of CYTOP CTL-809M (AGC Chemicals, Tokyo, Japan) was spun coated at 2000 rpm for 40 s and formed a ~1 μm thick CYTOP layer. Afterward, the sample was kept inside the desiccator overnight in order to remove any residual solvent. Then the Cu contact was made on top of the channel and a layer of Acrylic (MG Chemicals, Burlington, ON, Canada) was applied to seal the device.

The sample was characterized by scanning electron microscopy (SEM-Hitachi SU70) and X-ray diffraction (XRD-Bruker D8 Advance) methods. The I–V characteristics of the device were studied using a two-channel source measure unit (SMU) (Keithley 2602A, Cleveland, OH, USA). All the measurements under light were performed when the sample was illuminated by a solar simulator (RST 300S) at 80 mW/cm² optical power. A schematic of the device structure is illustrated in Figure 1.

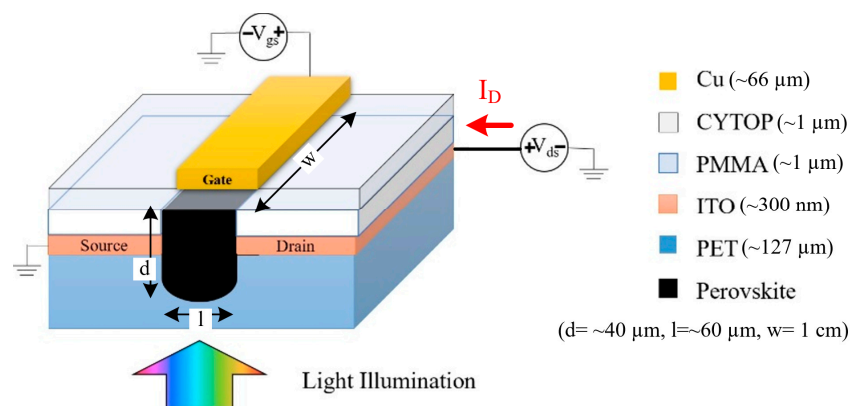


Figure 1. Schematic of the fabricated MAPbI₃ phototransistor.

3. Results and Discussion

The SEM image of the laser engraved channel is shown in Figure 2a. The channel width was measured to be $\sim 60 \mu\text{m}$. The crystallinity of the perovskite was then studied with the XRD method (Figure 2b). As reported in our previous work [34], it was a strong peak at 26.1° and a broad peak around 54° associated to the ITO coated PET substrate. Therefore, that part of the spectrum is not shown in Figure 2b. The two strong peaks at 2θ of 13.95° and 14.22° were assigned to (002) and (110) planes of tetragonal $\text{CH}_3\text{NH}_3\text{PbI}_3$ (space group $I4/mcm$) [31,32,35]. The XRD result also shows other crystalline orientations, which implies the formation of a polycrystalline structure in the channel.

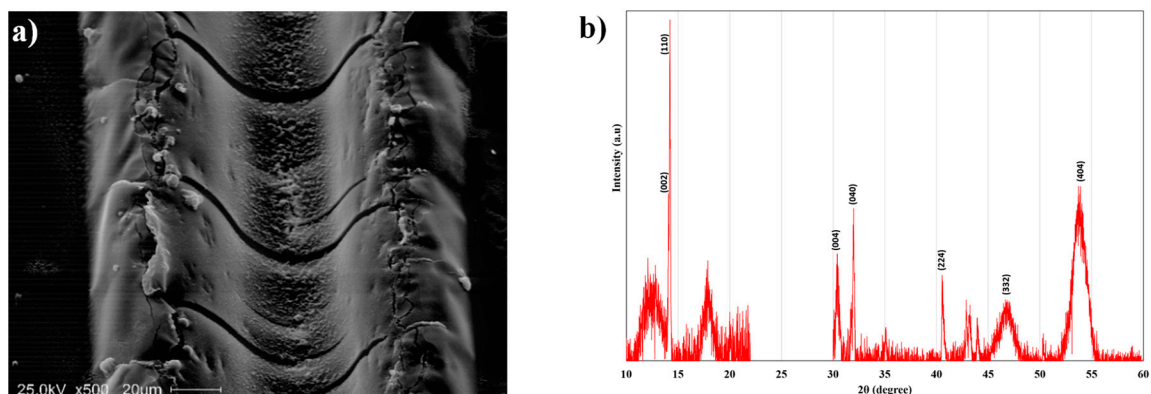


Figure 2. (a) The SEM image of the laser engraved microchannel (the image is taken at 44 degrees tilt angle), (b) the XRD spectra of the perovskite channel.

The transistor characteristics were measured in dark and under white light with the power density of $80 \text{ mW}\cdot\text{cm}^{-2}$. Since CYTOP surface hydrophobicity reduced at high electric fields [36] and may cause degradation of the perovskite layer, the output characteristics (drain current (I_D) versus drain voltage (V_{DS})) were measured from 0 V to 20.0 V while varying gate voltage (V_{GS}) from 10.0 V to 30.0 V by 10.0 V steps (Figure 3a,c). Additionally, the transfer characteristics (I_D versus V_{GS}) of the fabricated device were measured at V_{DS} of 20 V under light and dark conditions and are presented in Figure 3b,d, respectively. No significant changes were observed in the device characteristics after it was bent and relaxed. However, since our earlier studies showed the piezoelectric effect of the perovskite [35], no attempt was made to test the device when it was bent. Further characterization will be conducted and reported later to study the photo-piezo effect in the perovskite transistors.

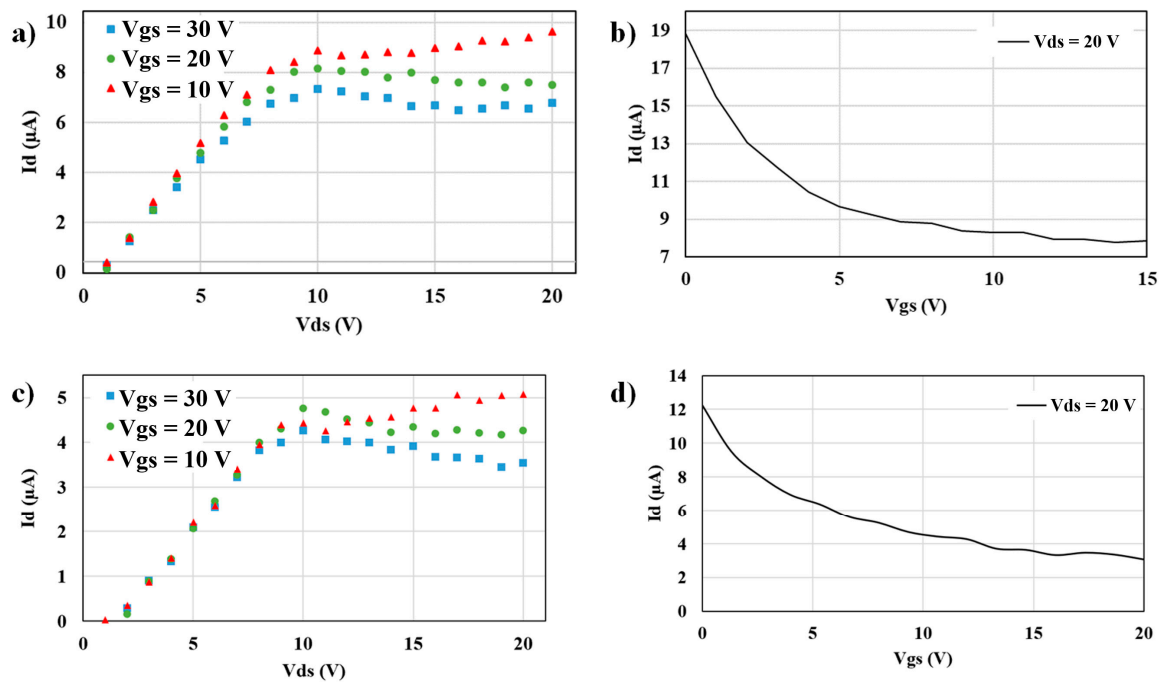


Figure 3. (a,c) Output and (b,d) transfer characteristics of the fabricated flexible photo-transistor (a,b) under light and (c,d) in dark.

As the channel was well encapsulated by CYTOP, all measurements were performed in ambient conditions. To minimize the ion-migration and bias stress effect, the overall time duration of each scan was set to ~ 8 s with a pause of a few minutes after each set of measurements while the sample was kept in the dark. In order to ensure that the current change was not the result of degradation of perovskite with time, the output characteristic measurements (Figure 3a,c) were repeated in reverse order as well (starting at V_{GS} of 30 V and decreasing down to 10 V) and the same trend was observed.

As shown in Figure 3a,c, the transistor reached the saturation region when the drain–source voltage was above 10.0 V. As the gate voltage increased, the saturated drain current decreased. The same trend was observed from the transfer characteristics both in dark and light conditions. The drain current dropped when the gate voltage increased at a drain voltage of 20.0 V which implies the depletion mode field-effect transistor (FET), not the enhancement. In fact, the non-zero current at $V_{GS} = 0$ V in the transfer characteristics (Figure 3b,d) confirms the depletion mode in which the transistor is normally “on”. Although the device showed a poor current modulation from the gate voltage, as shown in Figure 3, under illumination, the currents in both output and transfer characteristics were larger than the dark currents at the equal bias voltages. In Figure 3b,d at $V_{DS} = 20$ V when 0 V was applied to V_{GS} , the dark current was $I_D = 12.1$ μA . The current increased to 18.8 μA under illumination, showing a photocurrent of 6.7 μA (18.8 μA –12.1 μA). Considering the photoactive area of the transistor ($w \times l$ in Figure 1) and the intensity of the light (80 $\text{mW}\cdot\text{cm}^{-2}$), the photo-responsivity was estimated to be 14 $\text{mA}\cdot\text{W}^{-1}$, which is at least two orders of magnitude lower than the previously reported devices [17,37]. In this design, due to the high thickness of the channel (~ 40 μm) and the high optical absorption coefficient in MAPbI_3 (between 10^4 and 10^5 cm^{-1}) [38], light is not able to penetrate through the entire thickness of the semiconductor. Therefore, the top gate does not modulate the drain current effectively.

In addition to the thickness of the semiconductor, the polycrystalline structure of MAPbI_3 and the ion-migration in the material are limiting factors. The crystallization of grains at low temperatures by the solution-based fabrication process generates a large number of defects. These defects and trap states provide low activation energy and make a channel for the intrinsic migration of I^- , MA^+ , Pb^{2+} , and, in some cases, H^+ ions. These ions accumulate at the interfaces, screen the applied gate electric

field, and they can reduce the mobile electrons concentration in the accumulation layer of FET [39]. Therefore ion migration plays an important role in carrier transport in lead halide perovskite [40]. The concentration of carriers changes mobility [41,42].

Figure 4 represents the transfer characteristics of the device in dark. As the saturation current is in direct relation with the mobility, decreasing the mobility lower the saturation current. The mobility of the fabricated device was calculated to be $\sim 1.7 \text{ cm}^2 \cdot \text{V}^{-1} \cdot \text{s}^{-1}$ from the linear region of the transfer characteristic on using Equation (1).

$$\mu = \frac{l}{CwV_{ds}} \frac{\partial I_D}{\partial V_{gs}} \quad (1)$$

where, C is the capacitor of CYTOP layer estimated from the thickness of the dielectric and its relative permittivity, l is the channel length ($60 \mu\text{m}$), and w is the channel width (1 cm). Although a mobility higher than $100 \text{ cm}^2 \cdot \text{V}^{-1} \cdot \text{s}^{-1}$ has been reported in the bulk of a single crystalline perovskite [8], the reported field-effect mobility in perovskite-based transistors are in the range of $1\text{--}9 \text{ cm}^2 \cdot \text{V}^{-1} \cdot \text{s}^{-1}$ [26]. The visible defects in Figure 2a and the polycrystalline structure of perovskite (Figure 2b) suggest having relatively high density of traps that has a direct effect on the mobility. Additionally, it is likely that the negative charged point defects drifted toward the CYTOP/perovskite interface (with a positive gate voltage) and screened the applied gate electric field. This effect and the depletion mode operation of the FET due to the thick layer of the perovskite resulted in a unipolar p-type transport characteristic, as shown in the transfer characteristics. Table 1 is a summary of fabricated MAPbI₃-based phototransistors with some transistors showing ambipolar responses with the perovskite, acting as n-type and p-type semiconductors under negative and positive gate voltages, respectively.

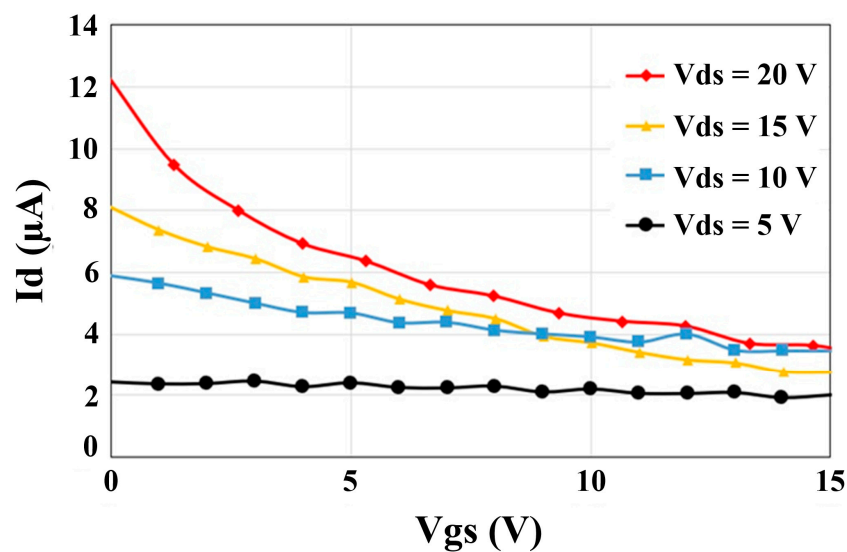


Figure 4. The transfer characteristics of the fabricated phototransistor in dark at different drain–source voltages.

The presented results here are promising for the fabrication of low-cost perovskite-based photodetectors. However, a modification in the design is required to make shallower micro-channels to obtain a thinner perovskite. It is expected that the current modulation and photo-response would be improved with a lower thickness of perovskite.

Table 1. Summary of fabricated MAPbI₃-based phototransistors.

Year	Material	Flexibility	Fabrication Method	Carrier Transport/Operational Temperature	Ref.
2015	MAPbI ₃ thin film	✗	Two-step vapor-assisted	Ambipolar	[17]
2015	MAPbI _{3-x} Cl _x		One-step spin coating	No current modulation	[15]
2015	Hybrid graphene MAPbBr ₂ I	✗	One-step spin coating	Ambipolar	[13]
2015	Tetragonal MAPbI ₃ thin film	✗	One-step spin coating	LT ** current modulation	[10]
2016	2D MAPbI ₃	✗	Combined solution process and vapor-phase conversion	No current modulation	[37]
2015	MAPbI ₃ micro-crystals	✗	Seeded growth process		[26]
2016	Hybrid C8BTBT * onto MAPbI ₃	✗	Co-evaporating	Unipolar	[14]
2016	MAPbI ₃	✗	Modified vapor-assisted solution process	Unipolar	[43]
2017	MAPbI ₃ thin film	✗	Doctor blade	No current modulation	[44]
2017	MAPbI ₃ microplates	✗	Vapor phase intercalation	LT current modulation	[18]
2017	Hybrid MAPbI _{3-x} Cl _x /CNT	✗	One-step spin coating	Ambipolar	[25]
2017	MAPbI ₃ thin film	✗	Two-step spin coating	No transfer characteristic	[22]
2017	MAPbI ₃ thin film	✗	One-step spin coating	Unipolar at HT ***	[39]
2018	MAPbI _x Cl _{3-x}	✗	Multi-step annealing process	No Saturation Regime	[23]
2018	MAPbI ₃ thin film	✗	One-step spin coating	Vertical structure with ITO contact	[45]
2019	MAPbI ₃ thin film	✗	One-step spin coating	Ambipolar	[20]
2019	MAPbI ₃ micro/nanowire	✗		Unipolar/P-type	[46]
2019	MAPbI ₃	✗	One-step spin coating	Ambipolar	[47]
2019	MAPbI ₃ thin film	✗	Hot-casting method	Unipolar/P-type	[24]
2019	MAPbI _x Cl _{3-x}	✗	One-step spin coating	Ambipolar	[12]
2020	MAPbI ₃ /PDVT-10 and MAPbI ₃ /N2200	✗	Cast and mold cleanroom microfluidic fabrication	Ambipolar	[48]
2020	MAPbI ₃	✓	Laser engraving + Capillary on Flexible substrate	Unipolar/P-type	This work

* Dioctylbenzothieno[2,3-*b*]benzothiophene, ** Low temperature, *** High temperature.

4. Conclusions

In this work, we introduced a new fabrication method to make an MAPbI₃ flexible phototransistor based on a lateral structure and top-gate contact configuration. Laser engraving was employed to make a microfluidic channel with the width of 60 μm on ITO coated PET substrate. The fabricated device operated in the triode and saturation regions in dark and under light illumination while showing p-type transport characteristics. This novel fabrication method provides a simple solution to make an MAPbI₃ transistor with comparably high mobility on flexible hydrophobic substrates.

Author Contributions: A.T. is the principal investigator (PI) of the project at USF. F.K. designed, fabricated, and characterized the fabricated device. Both authors contributed to writing the paper. All authors have read and agreed to the published version of the manuscript.

Funding: This research received no external funding.

Conflicts of Interest: The authors declare no conflict of interest.

References

- Zhu, H.; Shin, E.S.; Liu, A.; Ji, D.; Xu, Y.; Noh, Y.Y. Printable semiconductors for backplane TFTs of flexible OLED displays. *Adv. Funct. Mater.* **2020**, *30*, 1904588. [[CrossRef](#)]
- Haneef, H.F.; Zeidell, A.M.; Jurchescu, O.D. Charge carrier traps in organic semiconductors: A review on the underlying physics and impact on electronic devices. *J. Mater. Chem. C* **2020**, *8*, 759–787. [[CrossRef](#)]
- Petti, L.; Münzenrieder, N.; Vogt, C.; Faber, H.; Büthe, L.; Cantarella, G.; Bottacchi, F.; Anthopoulos, T.D.; Tröster, G. Metal oxide semiconductor thin-film transistors for flexible electronics. *Appl. Phys. Rev.* **2016**, *3*, 021303. [[CrossRef](#)]
- Ju, M.G.; Dai, J.; Ma, L.; Zeng, X.C. Perovskite chalcogenides with optimal bandgap and desired optical absorption for photovoltaic devices. *Adv. Energy Mater.* **2017**, *7*, 1700216. [[CrossRef](#)]

5. Jiang, Y.; Juarez-Perez, E.J.; Ge, Q.; Wang, S.; Leyden, M.R.; Ono, L.K.; Raga, S.R.; Hu, J.; Qi, Y. Post-annealing of MAPbI₃ perovskite films with methylamine for efficient perovskite solar cells. *Mater. Horizons* **2016**, *3*, 548–555. [[CrossRef](#)]
6. Djurišić, A.; Liu, F.; Tam, H.; Wong, M.; Ng, A.; Surya, C.; Chen, W.; He, Z. Perovskite solar cells—An overview of critical issues. *Prog. Quant. Electron.* **2017**, *53*, 1–37. [[CrossRef](#)]
7. Schuster, O.; Wientjes, P.; Shrestha, S.; Levchuk, I.; Sytnyk, M.; Matt, G.J.; Osvet, A.; Batentschuk, M.; Heiss, W.; Brabec, C.J. Looking beyond the surface: The band gap of bulk methylammonium lead iodide. *Nano Lett.* **2020**, *20*, 3090–3097. [[CrossRef](#)]
8. Dong, Q.; Fang, Y.; Shao, Y.; Mulligan, P.; Qiu, J.; Cao, L.; Huang, J. Electron-hole diffusion lengths >175 μm in solution-grown CH₃NH₃PbI₃ single crystals. *Science* **2015**, *347*, 967–970. [[CrossRef](#)]
9. Ava, T.T.; Al Mamun, A.; Marsillac, S.; Namkoong, G. A review: Thermal stability of methylammonium lead halide based perovskite solar cells. *Appl. Sci.* **2019**, *9*, 188. [[CrossRef](#)]
10. Chin, X.Y.; Cortecchia, D.; Yin, J.; Bruno, A.; Soci, C. Lead iodide perovskite light-emitting field-effect transistor. *Nat. Commun.* **2015**, *6*, 7383. [[CrossRef](#)]
11. Lin, Y.H.; Pattanasattayavong, P.; Anthopoulos, T.D. Metal-Halide Perovskite Transistors for Printed Electronics: Challenges and Opportunities. *Adv. Mater.* **2017**, *29*, 1702838. [[CrossRef](#)]
12. Zhou, Z.; Guo, N.; Peng, Y.; Tang, L.; Zhang, J.; Cai, H.; Ni, J.; Sun, Y.; Li, J. The Effect of Annealing Pressure on Perovskite Films and Its Thin-Film Field-Effect Transistors' Performance. *Phys. Stat. Solid. A* **2019**, *216*, 1900434. [[CrossRef](#)]
13. Wang, Y.; Zhang, Y.; Lu, Y.; Xu, W.; Mu, H.; Chen, C.; Qiao, H.; Song, J.; Li, S.; Sun, B. Hybrid graphene-perovskite phototransistors with ultrahigh responsivity and gain. *Adv. Opt. Mater.* **2015**, *3*, 1389–1396. [[CrossRef](#)]
14. Wang, J.; Liu, F.; Wang, G.; Wang, L.; Jiang, C. Novel organic-perovskite hybrid structure forward photo field effect transistor. *Organ. Electron.* **2016**, *38*, 158–163. [[CrossRef](#)]
15. Mei, Y.; Zhang, C.; Vardeny, Z.; Jurchescu, O. Electrostatic gating of hybrid halide perovskite field-effect transistors: Balanced ambipolar transport at room-temperature. *MRS Commun.* **2015**, *5*, 297–301. [[CrossRef](#)]
16. Lv, Q.; Wang, Z.; Dong, G.; Yan, Q. Anisotropic Carrier Transport in CH₃NH₃PbI₃ Single Crystal Field-Effect Transistor. *IEEE Electr. Dev. Lett.* **2018**, *39*, 1389–1392. [[CrossRef](#)]
17. Li, F.; Ma, C.; Wang, H.; Hu, W.; Yu, W.; Sheikh, A.D.; Wu, T. Ambipolar solution-processed hybrid perovskite phototransistors. *Nat. Commun.* **2015**, *6*, 8238. [[CrossRef](#)]
18. Li, D.; Cheng, H.C.; Wang, Y.; Zhao, Z.; Wang, G.; Wu, H.; He, Q.; Huang, Y.; Duan, X. The Effect of Thermal Annealing on Charge Transport in Organolead Halide Perovskite Microplate Field-Effect Transistors. *Adv. Mater.* **2017**, *29*, 1601959. [[CrossRef](#)]
19. Kagan, C.; Mitzi, D.; Dimitrakopoulos, C. Organic-inorganic hybrid materials as semiconducting channels in thin-film field-effect transistors. *Science* **1999**, *286*, 945–947. [[CrossRef](#)]
20. Ji, J.; Haque, F.; Hoang, N.T.T.; Mativenga, M. Ambipolar Transport in Methylammonium Lead Iodide Thin Film Transistors. *Crystals* **2019**, *9*, 539. [[CrossRef](#)]
21. Huo, C.; Liu, X.; Song, X.; Wang, Z.; Zeng, H. Field-effect transistors based on van-der-waals-grown and dry-transferred all-inorganic perovskite ultrathin platelets. *J. Phys. Chem. Lett.* **2017**, *8*, 4785–4792. [[CrossRef](#)]
22. He, B.; Li, W.; Wang, Q.; Liang, L.; Wang, H.; Xu, J.; Yang, S.; Jiang, Y.; Tang, Y.; Zou, B. Ultrasensitive all-solution-processed field-effect transistor based perovskite photodetectors with sol-gel SiO₂ as the dielectric layer. *J. Alloys Compd.* **2017**, *717*, 150–155. [[CrossRef](#)]
23. Cao, M.; Zhang, Y.; Yu, Y.; Jin, L.; Li, Y.; Chen, Z.; Che, Y.; Dai, H.; Zhang, G.; Yao, J. Enhanced perovskite phototransistor by multi-step slow annealing strategy. *Opt. Mater.* **2018**, *84*, 498–503. [[CrossRef](#)]
24. Canicoba, N.D.; Zagni, N.; Liu, F.; Mccuistian, G.; Fernando, K.; Bellezza, H.; Traore, B.; Rogel, R.; Tsai, H.; Le Brizoual, L. Halide Perovskite High-k Field Effect Transistors with Dynamically Reconfigurable Ambipolarity. *ACS Mater. Lett.* **2019**, *1*, 633–640. [[CrossRef](#)]
25. Li, F.; Wang, H.; Kufer, D.; Liang, L.; Yu, W.; Alarousu, E.; Ma, C.; Li, Y.; Liu, Z.; Liu, C. Ultrahigh Carrier Mobility Achieved in Photoresponsive Hybrid Perovskite Films via Coupling with Single-Walled Carbon Nanotubes. *Adv. Mater.* **2017**, *29*, 1602432. [[CrossRef](#)]
26. Wang, G.; Li, D.; Cheng, H.-C.; Li, Y.; Chen, C.-Y.; Yin, A.; Zhao, Z.; Lin, Z.; Wu, H.; He, Q. Wafer-scale growth of large arrays of perovskite microplate crystals for functional electronics and optoelectronics. *Sci. Adv.* **2015**, *1*, e1500613. [[CrossRef](#)] [[PubMed](#)]

27. Xie, C.; Liu, C.K.; Loi, H.L.; Yan, F. Perovskite-Based Phototransistors and Hybrid Photodetectors. *Adv. Funct. Mater.* **2019**, *30*, 1903907. [[CrossRef](#)]
28. Park, N.-G. Perovskite solar cells: An emerging photovoltaic technology. *Mater. Today* **2015**, *18*, 65–72. [[CrossRef](#)]
29. Kalaiselvi, C.; Muthukumarasamy, N.; Velauthapillai, D.; Kang, M.; Senthil, T. Importance of halide perovskites for next generation solar cells—a review. *Mater. Lett.* **2018**, *219*, 198–200. [[CrossRef](#)]
30. Khorramshahi, F.; Ghazizadeh, N.; Kymissis, I.; Takshi, A. Laser engraving method to fabricate iodide and bromide-based perovskite photosensors. In *Proceedings of Organic and Hybrid Sensors and Bioelectronics XIII*; SPIE: Bellingham, WA, USA, 2020; p. 114750L.
31. Khorramshahi, F.; Aljafari, B.; Kymissis, I.; Takshi, A. Laser assisted rapid fabrication of perovskite photodetector. In *Proceedings of Organic and Hybrid Sensors and Bioelectronics XII*; SPIE: Bellingham, WA, USA, 2019; p. 110960C.
32. Khorramshahi, F.; Takshi, A. Novel fabrication of flexible perovskite photosensor using capillary motion. In *Proceedings of Organic and Hybrid Sensors and Bioelectronics XI*; SPIE: Bellingham, WA, USA, 2018; p. 107380R.
33. Khorramshahi, F.; Takshi, A. Study of the stability of lead halide perovskite under two different fluoropolymer top coatings. *MRS Adv.* **2020**, *5*, 377–383. [[CrossRef](#)]
34. Khorramshahi, F.; Okeke, O.E.; Takshi, A. Electrochemical photocurrent enhancement in a ZnO-perovskite heterojunction using piezoelectric effect. *Electrochim. Acta* **2018**, *266*, 110–117. [[CrossRef](#)]
35. Khorramshahi, F.; Woughter, A.G.; Ram, M.K.; Kymissis, I.; Takshi, A. Apparent Piezo-Photocurrent Modulation in Methylammonium Lead Iodide Perovskite Photodetectors. *Adv. Electron. Mater.* **2019**, *5*, 1900518. [[CrossRef](#)]
36. Chae, J.B.; Kwon, J.O.; Yang, J.S.; Kim, D.; Rhee, K.; Chung, S.K. Optimum thickness of hydrophobic layer for operating voltage reduction in EWOD systems. *Sens. Actuat. A Phys.* **2014**, *215*, 8–16. [[CrossRef](#)]
37. Liu, J.; Xue, Y.; Wang, Z.; Xu, Z.-Q.; Zheng, C.; Weber, B.; Song, J.; Wang, Y.; Lu, Y.; Zhang, Y. Two-dimensional CH₃NH₃PbI₃ perovskite: Synthesis and optoelectronic application. *ACS Nano* **2016**, *10*, 3536–3542. [[CrossRef](#)]
38. Xing, G.; Mathews, N.; Sun, S.; Lim, S.S.; Lam, Y.M.; Grätzel, M.; Mhaisalkar, S.; Sum, T.C. Long-range balanced electron-and hole-transport lengths in organic-inorganic CH₃NH₃PbI₃. *Science* **2013**, *342*, 344–347. [[CrossRef](#)]
39. Senanayak, S.P.; Yang, B.; Thomas, T.H.; Giesbrecht, N.; Huang, W.; Gann, E.; Nair, B.; Goedel, K.; Guha, S.; Moya, X. Understanding charge transport in lead iodide perovskite thin-film field-effect transistors. *Sci. Adv.* **2017**, *3*, e1601935. [[CrossRef](#)]
40. Yuan, Y.; Huang, J. Ion migration in organometal trihalide perovskite and its impact on photovoltaic efficiency and stability. *Account Chem. Res.* **2016**, *49*, 286–293. [[CrossRef](#)]
41. Zhang, M.; Zhang, X.; Huang, L.-Y.; Lin, H.-Q.; Lu, G. Charge transport in hybrid halide perovskites. *Phys. Rev. B* **2017**, *96*, 195203. [[CrossRef](#)]
42. Bi, C.; Shao, Y.; Yuan, Y.; Xiao, Z.; Wang, C.; Gao, Y.; Huang, J. Understanding the formation and evolution of interdiffusion grown organolead halide perovskite thin films by thermal annealing. *J. Mater. Chem. A* **2014**, *2*, 18508–18514. [[CrossRef](#)]
43. Wu, Y.; Li, J.; Xu, J.; Du, Y.; Huang, L.; Ni, J.; Cai, H.; Zhang, J. Organic-inorganic hybrid CH₃NH₃PbI₃ perovskite materials as channels in thin-film field-effect transistors. *RSC Adv.* **2016**, *6*, 16243–16249. [[CrossRef](#)]
44. Tong, S.; Wu, H.; Zhang, C.; Li, S.; Wang, C.; Shen, J.; Xiao, S.; He, J.; Yang, J.; Sun, J. Large-area and high-performance CH₃NH₃PbI₃ perovskite photodetectors fabricated via doctor blading in ambient condition. *Organ. Electron.* **2017**, *49*, 347–354. [[CrossRef](#)]
45. Yu, H.; Cheng, Y.; Shin, D.; Tsang, S.W.; So, F. Vertical Organic-Inorganic Hybrid Perovskite Schottky Junction Transistors. *Adv. Electron. Mater.* **2018**, *4*, 1800039. [[CrossRef](#)]
46. Hong, Z.; Zhao, J.; Huang, K.; Cheng, B.; Xiao, Y.; Lei, S. Controllable switching properties in an individual CH₃NH₃PbI₃ micro/nanowire-based transistor for gate voltage and illumination dual-driving non-volatile memory. *J. Mater. Chem. C* **2019**, *7*, 4259–4266. [[CrossRef](#)]

47. Hoang, N.T.T.; Haque, F.; Ji, J.; Mativenga, M. Fast-Switching Mixed A-Cation Organic-Inorganic Hybrid Perovskite TFTs. *IEEE Electron. Device Lett.* **2019**, *40*, 917–920. [[CrossRef](#)]
48. Chen, P.-A.; Guo, J.; Nouri, M.; Tao, Q.; Li, Z.; Li, Q.; Du, L.; Chen, H.; Dong, Z.; Chang, L. Microfluidic Solution-Processed Organic and Perovskite Nanowires Fabricated for Field-Effect Transistors and Photodetectors. *J. Mater. Chem. C* **2020**, *8*, 2353–2362. [[CrossRef](#)]

Publisher’s Note: MDPI stays neutral with regard to jurisdictional claims in published maps and institutional affiliations.



© 2020 by the authors. Licensee MDPI, Basel, Switzerland. This article is an open access article distributed under the terms and conditions of the Creative Commons Attribution (CC BY) license (<http://creativecommons.org/licenses/by/4.0/>).